Weibull Wind-Speed Distribution Parameters Derived from a Combination of Wind-Lidar and Tall-Mast Measurements Over Land, Coastal and Marine Sites

Gryning, Sven-Erik; Floors, Rogier Ralph; Pena Diaz, Alfredo; Batchvarova, Ekaterina; Brümmer, Burghard

Published in:
Boundary-layer Meteorology

Link to article, DOI:
10.1007/s10546-015-0113-x

Publication date:
2016

Document Version
Publisher's PDF, also known as Version of record

Boundary-Layer Meteorol (2016) 159:329–348
DOI 10.1007/s10546-015-0113-x

ARTICLE

Weibull Wind-Speed Distribution Parameters Derived from a Combination of Wind-Lidar and Tall-Mast Measurements Over Land, Coastal and Marine Sites

Sven-Erik Gryning[1] · **Rogier Floors**[1] · **Alfredo Peña**[1] · **Ekaterina Batchvarova**[1,2] · **Burghard Brümmer**[3]

Received: 25 February 2015 / Accepted: 10 November 2015 / Published online: 27 November 2015

Abstract Wind-speed observations from tall towers are used in combination with observations up to 600 m in altitude from a Doppler wind lidar to study the long-term conditions over suburban (Hamburg), rural coastal (Høvsøre) and marine (FINO3) sites. The variability in the wind field among the sites is expressed in terms of mean wind speed and Weibull distribution shape-parameter profiles. The consequences of the carrier-to-noise-ratio (*CNR*) threshold-value choice on the wind-lidar observations are revealed as follows. When the wind-lidar *CNR* is lower than a prescribed threshold value, the observations are often filtered out as the uncertainty in the wind-speed measurements increases. For a pulsed heterodyne Doppler lidar, use of the traditional –22 dB *CNR* threshold value at all measuring levels up to 600 m results in a ≈7 % overestimation in the long-term mean wind speed over land, and a ≈12 % overestimation in coastal and marine environments. In addition, the height of the profile maximum of the shape parameter of the Weibull distribution (so-called reversal height) is found to depend on the applied *CNR* threshold; it is found to be lower at small *CNR* threshold values. The reversal height is greater in the suburban (high roughness) than in the rural (low roughness) area. In coastal areas the reversal height is lower than that over land and relates to the internal boundary layer that develops downwind from the coastline. Over the sea the shape parameter increases towards the sea surface. A parametrization of the vertical profile of the shape parameter fits well with observations over land, coastal regions and over the sea. An applied model for the dependence of the reversal height on the surface roughness is in good agreement with the observations over land.

Keywords Carrier-to-noise ratio · Doppler wind lidar · Reversal height · Shape parameter of the Weibull distribution · Wind profile

✉ Sven-Erik Gryning
sveg@dtu.dk

1 DTU Wind Energy, Technical University of Denmark, Risø Campus, Roskilde, Denmark

2 National Institute of Meteorology and Hydrology, Sofia, Bulgaria

3 Meteorological Institute, University of Hamburg, Hamburg, Germany

1 Introduction

The increase in wind-turbine height and the increase in area swept by the blades harvesting energy from airflow in the lower atmosphere have raised a need for better understanding of the structure of the vertical profile of the horizontal wind (Gryning et al. 2007), gusts (Suomi et al. 2015), and the monthly to annual long-term statistical distribution of boundary-layer winds (Gryning et al. 2014). Due to the strong non-linear relationship between wind speed and wind power, not only is an accurate description of the mean wind profile essential, but equally important is the description of its long-term variability for assessments of the wind-energy potential. Whereas the literature is rich in studies of the wind profile, investigations of its long-term variability are limited despite their obvious importance for wind-power assessments.

In connection with the development of wind power after the energy crisis in 1973, Justus and Mikhail (1976) suggested a parametrization of the wind-speed probability distribution in terms of the Weibull distribution, described by its scale and shape parameters. The parametrization was based on a universal power law of the vertical wind-speed profile proposed by Zimmer et al. (1975), but was limited to heights of 100 m and was soon found (Doran and Verholek 1978) to lead to significant errors. Based on a large number of measurements from land-based tall towers, Wieringa (1989) derived a simple empirical form for the vertical profile of the Weibull shape parameter over land that revealed many of the observed features, such as the height of the maximum in the shape parameter (reversal height), that had already been discussed much earlier by Hellmann (1917). The shape-parameter profile of Wieringa (1989) uses dimensional parameters and contains a site-dependent dimensional constant; he pointed out that the parametrization was limited by the data available at the time, especially concerning the profile of the shape parameter above the reversal height. By use of heterodyne detection Doppler lidar measurements, Gryning et al. (2014) proposed a parametrization that is also applicable well above the reversal height. In connection with the development of the European Wind Atlas, Troen and Petersen (1989) devised an expression for the reversal height by perturbing the geostrophic drag law used in connection to wind-resource assessments.

The Doppler wind-lidar technique is under rapid development, with measurements currently reaching several km in altitude under favourable conditions (O'Connor et al. 2010; Floors et al. 2013; Peña et al. 2013). However, the quality and height range of the wind observations depend on the strength of the backscattered signal compared to the noise signal, the so-called carrier-to-noise ratio (*CNR*). The *CNR* of lidars is discussed in general by Fujii and Fukuchi (2005) and for pulsed wind lidars by Cariou (2013). Frehlich (1996) argued that if the *CNR* falls below a prescribed threshold (he recommended $CNR > -22$ dB), the uncertainty in the wind speed is too large for the measurements to be useful. Floors (2013) and Peña et al. (2013) found good agreement between wind lidar and cup-anemometer measurements at 100 m for wind-lidar data filtered with $CNR > -22$ dB and deteriorated agreement for decreasing *CNR* thresholds.

The combination of tall-mast and wind-lidar long-term data over different underlying surfaces allows study of: (1) the wind-lidar data as a function of *CNR*, (2) the consequences of the choice of the *CNR* threshold value on the wind speed, the Weibull shape-parameter profile and the reversal height, and (3) parametrizations of the shape-parameter profile and the reversal height. Section 2 presents the experimental set-up, and in Sect. 3 the Weibull distribution and parameterizations are introduced. Section 4 gives illustrative examples on the consequences for the statistics of the wind speed and the reversal height when applying a different *CNR* threshold on the measurements. Finally, in Sect. 5, similarities and differences in the Weibull

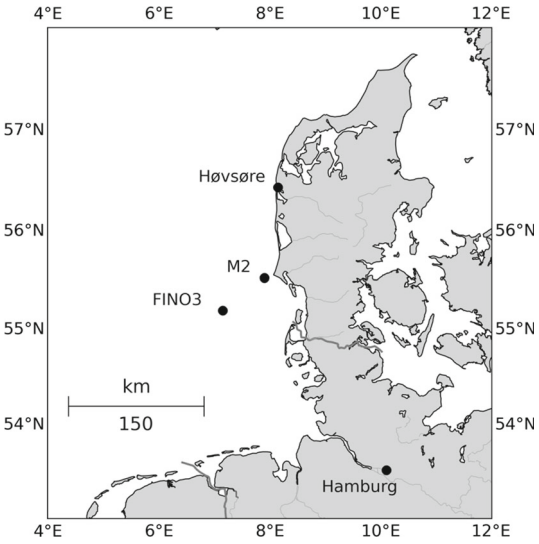

Fig. 1 Map showing the position of the three main measuring sites and the secondary site M2; land is marked in *grey* and water marked in *white*

distribution shape parameter and reversal height over land and at locations influenced by the sea are illustrated and discussed. Section 6 presents discussion and conclusions.

2 Wind Observations

The analyses herein are based on wind-lidar datasets from three sites: a suburban site near Hamburg, Germany; a coastal farmland at Høvsøre on the west coast of Denmark; and a marine site in the North Sea (FINO3). At these sites the wind-lidar observations were complemented with observations from tall meteorological masts. In addition, wind-profile measurements from a fourth site, a marine meteorological mast (M2) in the North Sea, are also used. Figure 1 shows the locations of the sites.

2.1 Hamburg (Suburban)

The 280-m high Hamburg weather mast is operated by the Meteorological Institute of the University of Hamburg. The meteorological facility is installed at the broadcasting tower of the Norddeutscher Rundfunk (NDR) at the eastern edge of Hamburg (53.5192°N, 10.1029°E) at a distance of about 8 km from the city centre. The Hamburg weather mast facility is described in detail in Brümmer et al. (2012) and Brümmer and Schultze (2015), thus, we give only a short description here. The entire facility consists of two parts: a 12-m mast and the main broadcasting mast; they are about 170 m apart. The 12-m mast is equipped at a height of 10 m with a three-dimensional sonic anemometer (Metek) for wind and turbulent flux measurements. Identical sonic anemometers are installed at the main mast at heights of 50, 110, 175, and 250 m on 5.5-m long booms (6.5 m from the mast centre) protruding into a direction of 190°. The sonic data are sampled at 20 Hz and routinely averaged to 1-, 5-, 10- and 60-min means; herein, we use the 10-min means. By fitting a logarithmic wind profile to the wind-speed measurements at all five levels between 10 and 250 m under neutral stability conditions, Konow (2014) estimated the aerodynamic roughness length (z_0) for different flow directions. She found that the roughness values range between 0.3 m for

the more rural easterly sectors and 1.2 m for the more industrial/sub-urban westerly sectors of the Hamburg weather mast. Gryning et al. (2007) found the overall roughness length to be ≈0.65 m in agreement with the roughness length of ≈0.6 m that was reported by Gryning and Lyck (1984) for sub-urban part of Copenhagen. The wind lidar was operated near the 12-m mast during the period 15 June 2011 to 23 March 2012.

2.2 Høvsøre (Both Land and Coastal)

The 116-m tall meteorological mast, part of the Danish National Test Station of wind turbines, is situated in a coastal rural farmland area in Jutland, consisting of grassland (Peña et al. 2015a). The mast (56°26′26.0″N; 08°09′03.1″E) is located 1.8 km east of the North Sea coastline and 200 m south of the closest wind-turbine stand. At the site the upwind land conditions can be considered as flat and homogeneous for easterly (Peña et al. 2015b), and typical coastal for westerly flows. Cup anemometers measure wind speed at heights of 2, 10, 40, 60, 80, 100 and 116 m at a mast, and at 160 m at a nearby light tower, and wind vanes measure the wind direction at 10, 60, 100 at the mast and 160 m at the light tower. The z_0 value of the rural area is about 0.01–0.02 m (Gryning et al. 2007; Blatt 2010). Wind-lidar measurements were performed during the period 23 April 2010 to 31 March 2011, and for this analysis, data from the azimuthal sector 045°–135° are taken to represent homogeneous upwind land conditions (Høvsøre-land) and data from the azimuthal sector 225°–315° to represent coastal conditions (Høvsøre-coastal).

2.3 FINO3 (Marine)

FINO3 is a German research platform in the North Sea (55.19501°N; 7.15836°E), 80 km west of the Danish island of Rømø. Meteorological measurements are performed on a lattice mast with booms between 30 and 105 m above mean sea level (m.s.l.). Prior studies have revealed that the mast distorts the flow in certain directions, and so three levels (50, 70 and 90 m) are equipped with cup anemometers on booms for each of the directions 105°, 225° and 345°, giving a less disturbed dataset. Additionally, the wind direction is measured at 28 and 100 m with wind vanes. The wind lidar was installed on the working platform at 24.5 m above m.s.l. and measurements were performed from 29 August 2013 to 26 June 2014.

2.4 M2 (Marine)

The M2 meteorological mast (55°31′08.8″N; 07° 47′15.1″E) has a lattice structure and is instrumented with cup anemometers at 15, 30 and 45 m, giving wind speeds closer to the sea surface compared to FINO3. The booms are directed towards the south-west and north-east at each level, giving a dataset that is nearly undisturbed by the mast. Wind direction is measured at 28 and 43 m. The operation of the cup anemometers and wind vanes started on 14 May 1999. In this study, only data from the start until the end of 2001 are used in order to ensure that the measurements are undisturbed by the nearby Horns Rev wind farm, which became fully operational in December 2002.

2.5 Wind Lidar

During the measurement campaigns at Hamburg, Høvsøre and FINO3 a pulsed heterodyne detection Doppler wind lidar (Leosphere WLS70) was operated near the meteorological masts (Cariou 2013). The wind lidar measured the radial wind-velocity components in four

azimuth angles separated by 90° at a zenith angle of 15°. Starting from 100 m in altitude, the 10-min averaged horizontal wind-velocity components are obtained with 50-m vertical resolution up to 2 km. Gryning et al. (2014) provide details on the wind lidar and its operation during the campaigns.

Lidar data quality is specified in terms of the *CNR*, which, following Fujii et al. (1978), Fujii and Fukuchi (2005) and Cariou (2013), is the strength of the heterodyne signal relative to the level of noise. For a very weak signal, velocity estimates are dominated by noise and thus subject to estimation errors. If the *CNR* falls below a predetermined threshold, Frehlich (1996) argues that the uncertainty in the velocity is deemed too large for the data to be useful. Thus, it is common practice to filter out measurements for this type of lidar when $CNR < -22$ dB (Aitkin et al. 2012) and the consequences of filtering the data with a certain *CNR* value are discussed below. The four most significant atmospheric factors influencing wind-lidar performance are aerosol backscatter, atmospheric refractive turbulence, relative humidity and precipitation (Aitkin et al. 2012). The *CNR* is linearly proportional to the aerosol backscatter and inversely proportional to the square of the propagation distance. Therefore, data availability decreases with range when using the same *CNR* value to filter the measurements. The wind-lidar performance is adversely affected by precipitation, as the radial Doppler velocity measurement includes a component of the raindrop fall velocity in addition to the air motion, which can significantly affect the calculation of horizontal wind speeds.

The wind-lidar profile data were analyzed up to 600 m in order to ensure a sufficiently large dataset for the analysis. A full profile is identified when the *CNR* values of concurrent measurements at all levels from 100 to 600 m are above a threshold values. Measuring periods are summarized in Table 1 and monthly data coverage is illustrated in Fig. 2.

3 Weibull Distribution and Reversal Height

In wind-power meteorology, the two-parameter Weibull distribution is often used to describe the long-term frequency distribution of the horizontal wind speed (Troen and Petersen 1989), because it both provides a good fit to wind-speed measurements and is mathematically easy to use. The two-parameter Weibull distribution probability density function $f_u(u)$ applied to the wind component u reads,

$$f_u(u) = \frac{k}{A}\left(\frac{u}{A}\right)^{k-1} \exp\left(-\left(\frac{u}{A}\right)^{k}\right), \tag{1}$$

where A is the scale parameter (units of speed) and k is the shape parameter (dimensionless). The Weibull distribution is typically applied to the 10-, 30-min or 1-h mean wind speed. Justus et al. (1978) summarize several methods to derive A and k. From the relationship between A, k, and the average wind speed $\langle u \rangle$,

$$\langle u \rangle = A\,\Gamma\,(1 + 1/k)\,, \tag{2}$$

where Γ is the Gamma function and $\langle \cdot \rangle$ denotes averaging, A is about 10 % larger than $\langle u \rangle$ for values of k typical for atmospheric conditions and thus the vertical profiles of A and $\langle u \rangle$ resemble each other. The vertical profile of the shape parameter is closely related to the profile of the standard deviation of the wind speed σ,

$$k = \left(\frac{\sigma}{\langle u \rangle}\right)^{-1.086}, \tag{3}$$

for $1 \leq k \leq 10$ where $\sigma^2 = \langle (u - \langle u \rangle)^2 \rangle$.

Table 1 Number of 10-min averaged measurements and measuring periods at each site

Site	Period	Anemometer measurements, assumed 100 %	Wind-lidar number at 100 m/ full profiles	Concurrent anemometer and wind-lidar measurements; full profiles
Høvsøre land sector (45–135°)	25 April 2010–31 March 2011	11,758	9885/8876 (84 %) / (75 %)	8754 (74 %)
Høvsøre coastal sector (225–315°)		17,377	12,618/11,616 (73 %)/(67 %)	11,383 (66 %)
Hamburg	15 June 2011–23 March 2012	39,374	34,692/27,504 (88 %)/(70 %)	26,403 (67 %)
FINO3	29 August 2013–26 June 2014	40,541	40,685/34,487 (100 %)/(85 %)	32,425 (80 %)
M2	14 May 1999–31 December 2001	136,646	Wind lidar was not installed	

The numbers in brackets represent the number of all wind-lidar measurements ($CNR > -35$ dB) relative to the total number of cup/sonic-anemometer measurements. A full profile is identified when $CNR > -35$ dB for the concurrent measurements at all levels from 100 to 600 m

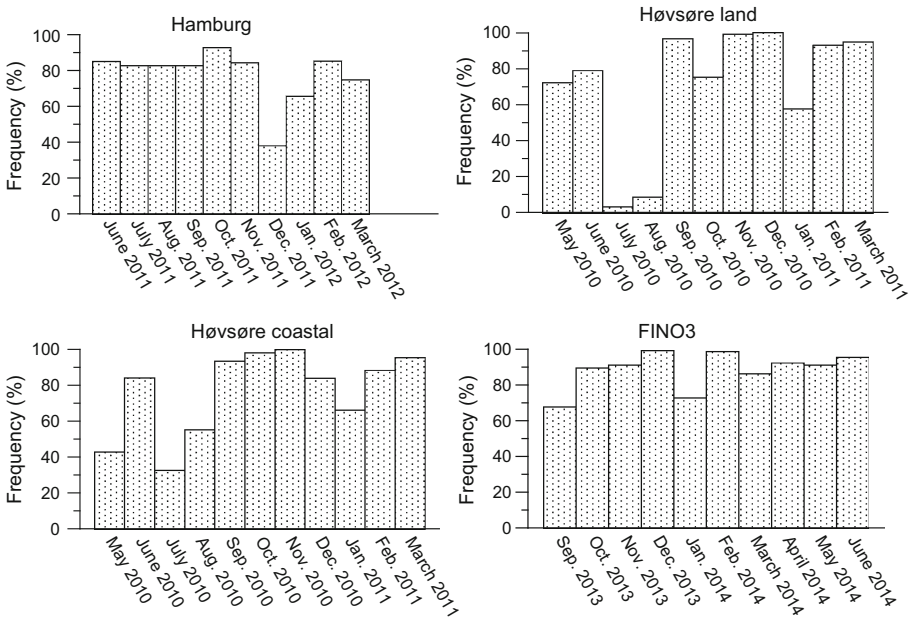

Fig. 2 Monthly data coverage for $CNR > -35$ dB of the 10-min averaged observations at 100 m from the wind lidar at Hamburg, Høvsøre land, Høvsøre coastal and FINO3. At Høvsøre land and coastal 100 % corresponds to the number of wind-vane observations at 100 m in the respective sector

Over land, the shape parameter increases from its value near the ground, reaches a maximum at the so-called reversal height, and then decreases towards its synoptic value in the free atmosphere. Although this distinct behaviour was already noticed by Hellmann (1917), it has received little attention in the literature. The reversal height is related to the combined effect of the diurnal variation in the local meteorological conditions and the variability of the synoptic conditions in the region. The nighttime stably-stratified layer near the ground reduces the vertical momentum exchange, thus decoupling it from the flow above and causing decreased wind speeds. The overlying wind speed increases because of the inhibited transfer of momentum to the lower stable layer (Brümmer and Schultze 2015). During daytime unstable conditions the vertical exchange of momentum is significant throughout the depth of the boundary layer.

However, over the North Sea, there is little diurnal variability in the surface fluxes. Changes in the heat flux and boundary-layer height are more related to synoptic influences, e. g. wind direction, than any diurnal variation (Floors 2010; Sathe et al. 2011). Cold-air flow from the north creates a deep and unstable boundary layer (Vincent et al. 2012) while relatively warm air of southerly origin leads to a stable or near-neutral, shallow marine boundary layer. Somewhat similar conditions with long-lived boundary layers exist in the High Arctic during both the long winter and summer, e.g. at Station North, Greenland (Batchvarova et al. 2014). Under such conditions it is expected that the shape parameter increases towards the surface.

For all sites, we study the profiles of the Weibull-distribution parameters and apply common parametrizations for the profile of the shape parameter and the reversal height. Gryning et al. (2014) suggest a parametrization of the vertical profile of the shape parameter as

$$k = k_\mathrm{s} + \underbrace{c\frac{z - z_\mathrm{s}}{z_\mathrm{r} - z_\mathrm{s}} \exp\left(-\frac{z - z_\mathrm{s}}{z_\mathrm{r} - z_\mathrm{s}}\right)}_{I} - \underbrace{(k_\mathrm{s} - k_\mathrm{t}) \exp\left(-\frac{z_\mathrm{t} - z_\mathrm{s}}{z - z_\mathrm{s}}\right)}_{II}, \tag{4}$$

where k_s is the value of the shape parameter at height z_s near the ground, z_r is the height of the shape-parameter maximum (reversal height), and k_t is related to the value in the upper part of the layer at height z_t, c is a dimensionless parametrization constant. The increase in k from its value near the ground until it reaches the reversal height is modelled by term I, which is a normalized version of the parametrization originally proposed by Wieringa (1989), while term II parametrizes the asymptotic approach of k above the reversal height in the upper part of the planetary boundary layer.

A simple model for the reversal height was proposed by Troen and Petersen (1989). The starting point is the geostrophic drag law in combination with the traditional logarithmic wind profile. Their derivation is based on a first-order expansion in the surface heat flux in the geostrophic drag law, giving a simple approximation to the reversal height,

$$\frac{z_r}{z_0} = \alpha \, Ro^{\beta}, \tag{5}$$

where α is a constant of proportionality and β is dimensionless. The surface Rossby number $Ro = G/fz_0$ is composed of the geostrophic wind speed G, the Coriolis parameter f, and the aerodynamic roughness length z_0. Combining Eqs. 5 and 6 gives

$$z_r = \alpha \left(\frac{G}{f}\right)^{\beta} z_0^{1-\beta} \tag{6}$$

The applicability of Eqs. 4 and 6, based on the measured k profile, is discussed in Sect. 5 for different *CNR* threshold values.

4 Lidar *CNR* Threshold

The analysis of the shape parameter and the reversal height is based on all available concurrent measurements of the complete wind profile, i.e. lidar profiles with *CNR* values larger than a given threshold at all measurement levels up to 600 m, combined with mast measurements (Table 1). The internal configuration of the wind lidar sets the minimum *CNR* threshold for recording measurements to –35 dB. In order to secure high quality data, it is customary to select measurements above a higher *CNR* threshold, traditionally *CNR* > –22 dB for this type of lidar.

The *CNR* depends not only on the characteristics of the specific wind lidar, but also on the size and concentration of atmospheric particles responsible for the backscattered signal. Lidars deployed at sites with low concentrations of aerosols are therefore likely to retrieve data with generally lower *CNR* values. This aspect is illustrated in Fig. 3 for the three wind-lidar sites (Hamburg, Høvsøre, and FINO3). Availability of 50 % of full wind-lidar profiles up to 600 m is obtained at a threshold *CNR* value of about –24 dB for the land sites (Hamburg and Høvsøre-land), and for the marine sites –22 dB (FINO3) and –19 dB (Høvsøre-coastal).

Figure 4 (left panel) illustrates an example from the Hamburg site of the sensitivity of the mean wind speed to the *CNR* threshold value. The selection of a high *CNR* threshold favours higher mean wind speeds throughout the layer and larger standard deviations. Figure 4 (right panel) shows the mean wind speed at 100 m for all wind-lidar sites (Hamburg, Høvsøre-land, Høvsøre-coastal and FINO3) as a function of the *CNR* value. It can be seen that the choice of threshold for *CNR* has a significant consequence for the derived mean wind speed. Choosing high quality measurements with a high value of *CNR* implies that predominantly high speed measurements are selected. Using –22 dB as a lower limit for *CNR*, results in a 7 % overestimation of the long-term mean wind speed at 100 m at the land sites, and a 12 %

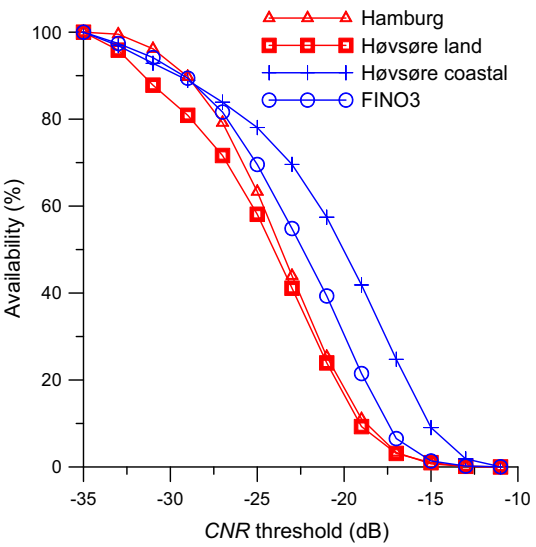

Fig. 3 Availability of full wind-lidar profiles as a function of the *CNR* threshold value. A full profile is identified when the *CNR* of the concurrent measurements at all levels between 100 and 600 m is above the threshold value; 100 % availability thus corresponds to the number of full profiles

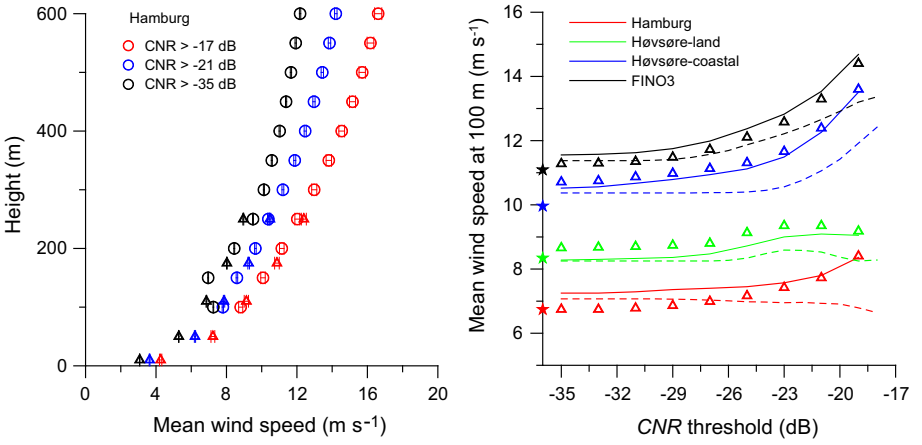

Fig. 4 The *left panel* shows the wind-speed profile at Hamburg; *circles* represent observations by the wind lidar for *CNR* threshold values of –17, –21 and –35 dB, respectively. *Triangles* represent concurrent data from anemometers. The *bars* represent the standard deviation of the mean wind speed. The *right panel* illustrates the mean wind speed at 100 m as a function of the *CNR* threshold value. The *full lines* are derived by filtering the wind-lidar measurements with the same *CNR* threshold value imposed at all levels from 100 to 600 m, *triangles* are the concurrent wind-speed values derived from the anemometer observations. The *dashed lines* are derived by filtering the wind-lidar measurements with the *CNR* threshold value at 100 m only. The *stars* are the mean wind speeds at 100 m that were derived from the anemometer observations at the meteorological masts when using all available measurements. Note: the measurements at Hamburg (mast 110 m and wind lidar 100 m) and FINO3 (mast 90 m and wind lidar 124 m) are derived for a height of 100 m by logarithmic interpolation

overestimation at the coastal and marine sites compared to the results when using a threshold of –35 dB.

When the *CNR* value of the wind-lidar measurements at 100 m was used for data filtering, and not imposed on the full profile up to 600 m, the relationship between the *CNR*

Table 2 Comparison between anemometer (Y) and lidar measurements (X) of the wind speed at 100 m at the Høvsøre and Hamburg* sites for different *CNR* thresholds. The comparison is illustrated by the bias ($\langle Y\rangle - \langle X\rangle$) where a bracket denotes an average; normalized bias 100 ($(\langle Y\rangle - \langle X\rangle)/\langle X\rangle$); root-mean-square error $RMSE = \sqrt{\sum_{i=1}^{N}(Y_i - X_i)^2/N}$; and mean absolute error $MAE = \sum_{i=1}^{N}|Y_i - X_i|/N$ where N is the number of samples

Site	*CNR* (dB)	Bias (m s^{-1})	Normalized bias (%)	*RMSE* (m s^{-1})	*MAE* (m s^{-1})
Høvsøre, coastal and land sectors	−35	0.22	2.4	0.62	0.42
	−25	0.22	2.3	0.59	0.41
	−20	0.13	1.2	0.43	0.31
	−15	0.04	0.3	0.40	0.27
Høvsøre land sector	−35	0.35	4.3	0.78	0.53
	−25	0.34	4.1	0.73	0.50
	−20	0.17	2.1	0.47	0.33
	−15	0.12	1.4	0.50	0.33
Høvsøre coastal sector	−35	0.19	1.8	0.46	0.32
	−25	0.19	1.8	0.46	0.32
	−20	0.15	1.3	0.36	0.27
	−15	0.09	0.7	0.35	0.25
Hamburg	−35	−0.15	−2.2	0.98	0.72
	−25	−0.06	−0.9	0.84	0.61
	−20	0.14	2.0	0.66	0.49
	−15	0.19	3.1	0.65	0.48

* In Hamburg sonic anemometer measurements were performed at 110 m and the lidar measurements at 100 m. It should be noted that the mast and wind lidar at the Hamburg site were positioned 170 m apart, which partly may explain the large *RMSE* and *MAE*. Similar numbers for FINO3 are not available due to the large difference in height between the upper cup anemometer (90 m) and the lower wind-lidar observation (124 m)

and the wind speed is illustrated by the dashed lines in Fig. 4 (right panel). Use of a *CNR* threshold value of –22 dB in these cases results in an overestimation of the long-term wind speed of 9 % in the marine environment (FINO3) and 4 % or less at the other sites.

The effect of the choice of *CNR* threshold on the statistics of the inter comparison of lidar and anemometer wind speeds at 100 m is given in Table 2. In general, the statistical metric decrease for increasing *CNR*. It is not only the estimated mean wind speed that is affected by the choice of *CNR* threshold, but also the profile of the shape parameter and the corresponding reversal height. This is illustrated in Fig. 5 (left panel) for the Hamburg site; the k parameter, its standard deviation and the reversal height decrease when lowering the *CNR* threshold. Figure 5 (right panel) shows that there is a weak effect on z_r at Høvsøre-coastal for a *CNR* threshold below –22 dB and the effect is pronounced at both Høvsøre-land and Hamburg. The reversal height over land is related to the diurnal variability of the wind speed. A high *CNR* threshold favours the selection of high wind speeds, which leads to higher reversal heights. The FINO3 marine site is not included in Fig. 5 because a reversal height cannot be identified from the measurements, an outcome suggested earlier when introducing Eq. 4.

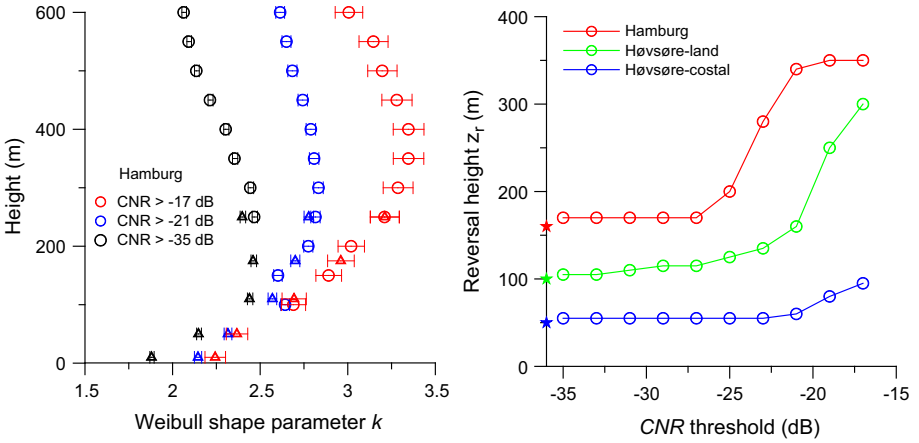

Fig. 5 The *left panel* shows profiles of the shape parameter k at Hamburg. The *circles* represent observations by the wind lidar for *CNR* threshold values of –17, –21 and –35 dB, respectively. *Triangles* represent concurrent data from anemometers. The *bars* represent the standard deviation. The *right panel* illustrates the reversal height as a function of the *CNR* threshold value, derived from the wind-lidar observations at Hamburg, Høvsøre-land and Høvsøre-coastal. The *stars* are the reversal heights that were derived from the anemometer observations at the meteorological masts when using all available measurements

5 Weibull Distribution Analysis

In the analysis of the Weibull distribution all concurrent and complete profiles of the wind speed up to 600 m with a $CNR > -35$ dB were used. The scale and shape parameter and the 68 % confidence limits (corresponding approximately to two standard deviations) were calculated from the long-term measurements of the wind speed by use of the maximum likelihood method (Bickel and Doksum 2001). Figure 6 provides an example of wind-speed histograms and the corresponding fitted Weibull distributions as function of height, based on measurements from the offshore FINO3 platform, and in Fig. 7 for the Hamburg and Høvsøre sites at 100 m.

5.1 Shape-Parameter Analysis

Here, we focus on the vertical profile of the shape parameter with Fig. 8 (upper panels) showing the shape parameter for the two inland sites, Hamburg and Høvsøre-land. The vertical profiles representing land conditions show a very pronounced maximum in the shape parameter at 100 to 200 m above the ground; greater at Hamburg than at Høvsøre-land. Figure 9 (upper panels) shows the shape parameter for Høvsøre-coastal and the marine boundary layer at FINO3. The k profile for the coastal sector at Høvsøre, expected to experience the transition from marine to land conditions for flow inland from the sea, reveals a maximum at a much lower level. Figure 9 (upper right panel) illustrates that, in the marine environment, the vertical profile of the shape parameter continuously decreases from the lowest measuring point upward. The lowest part of the profile increases almost linearly towards the sea surface, suggesting that the reversal height, if different from zero, is well below 50 m. In order to further investigate the behaviour of the shape parameter near the sea surface, measurements from a nearby marine meteorological mast (M2) were analyzed. At the M2 site, located 37 km east and 34 km north of the FINO3 platform (Fig. 1), measurements of wind speed indicate

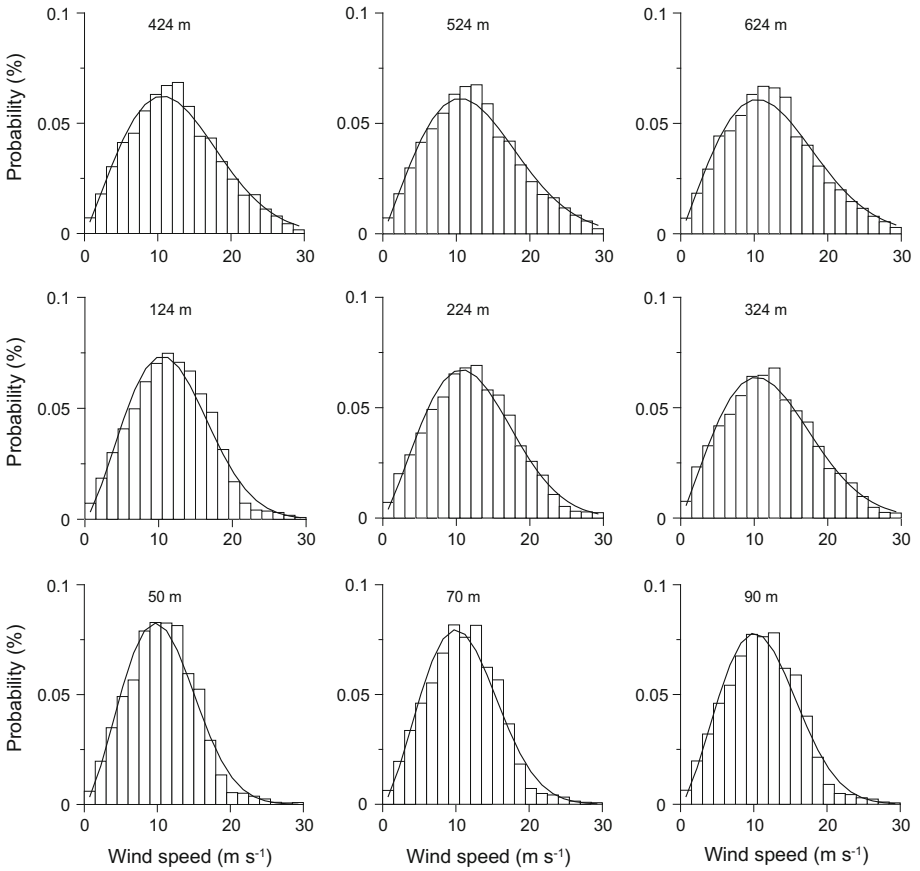

Fig. 6 Illustration of wind-speed histograms and fitted Weibull distributions for the measurements at the FINO3 platform between 50 and 624 m. The root-mean-square error between the histogram and fit of the Weibull distribution ranges from a maximum of 0.005 to a minimum of 0.003

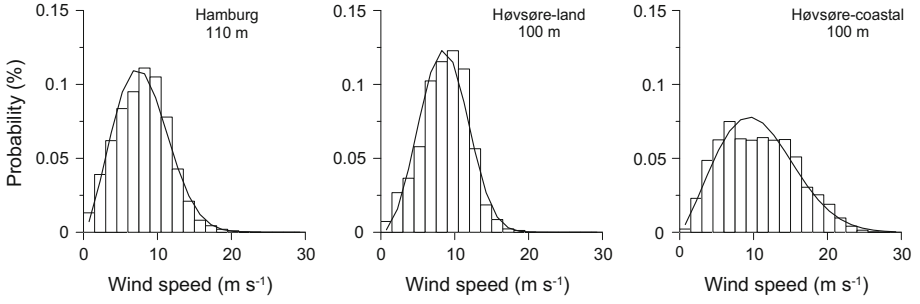

Fig. 7 Same as for Fig. 6 but for the measurements at Hamburg (110 m), Høvsøre-coastal (100 m) and Høvsøre-land (100 m). The root-mean-square error between the histogram and fit of the Weibull distribution ranges from 0.003 to 0.011, 0.004 to 0.011 and 0.004 to 0.008 for the profiles at Hamburg, Høvsøre-land and Høvsøre-coastal, respectively

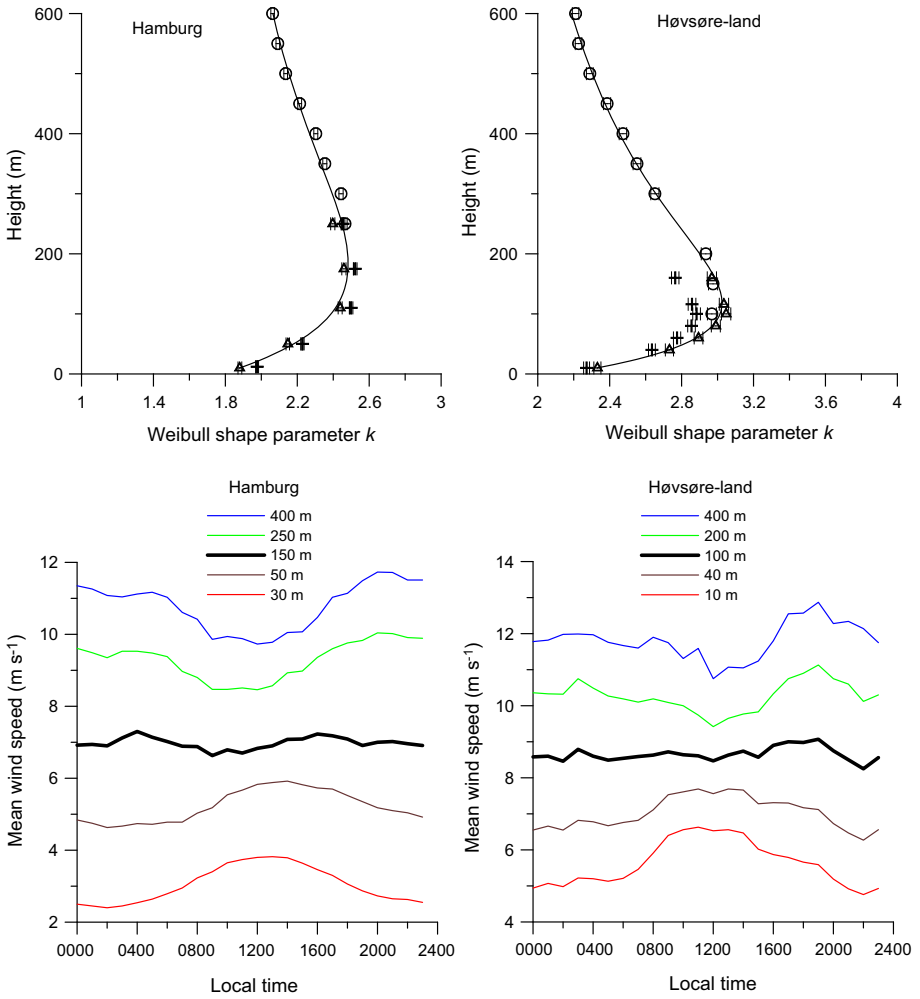

Fig. 8 *Upper panels* show k profiles for the land sites. *Circles* represent observations from the wind lidar, *triangles* from concurrent anemometer measurements and the crosses from all available anemometer measurements. The *bars* represent the standard deviation. The full line is the fit taken from Eq. 4. *Lower panels* illustrate the daily variability of the wind speed as function of height for the same sites and measuring periods. The *highlighted black line* shows the wind variability at approximately the reversal height

that the shape parameter continues to increase towards the sea surface from 45 to 30 m and that there is no clear trend observable between the 30- and 15-m levels.

The solid line for the k profiles in Figs. 8 and 9 represents a least-squares fit (Coleman and Li 1996) to k profiles by using Eq. 4; results are given in Table 3. The crosses represent the k profiles derived from all available mast measurements. It can be seen that the two sets of measurements agree well in Hamburg and show smaller k values when analyzing all mast measurements at Høvsøre and FINO3. To illustrate the connection between wind speed and the profiles of the shape parameter, the diurnal variation of the mean wind speed at a number of heights is shown in the lower panels of Figs. 8 and 9. We recall that the reversal height (the maximum in the k profile) is the level with a minimum in the variability of the long-term

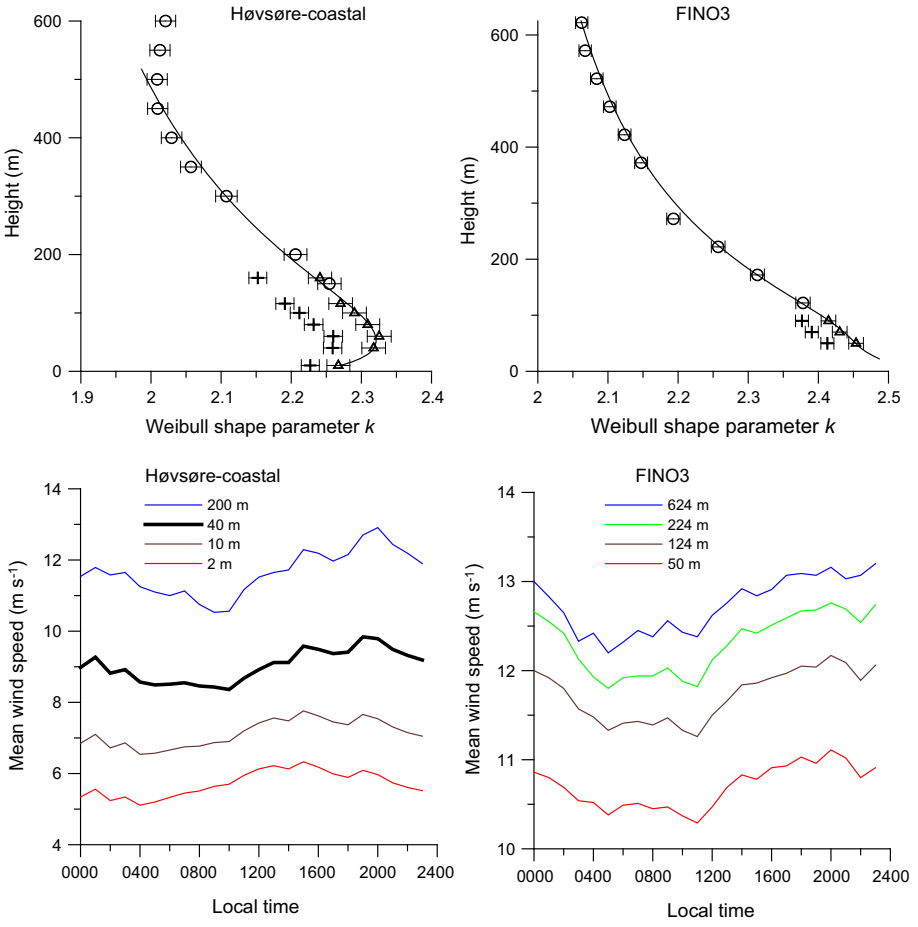

Fig. 9 Same as for Fig. 8 but for the coastal (*left panels*) and marine (*right panels*) sites

wind speed. It can be seen that near the surface over land the mean wind speed is low during the night and high during the day. At about a height of 100 m at Høvsøre-land and 150 m at Hamburg, there is little variation in the wind speed between day and night, and above these layers the wind speed behaviour is reversed, the wind speed being higher during the night. This is in good agreement with the estimated reversal height in the k profile for the two land sites. A similar behaviour has been reported in Petersen (1975) and Brümmer et al. (2012).

For the coastal sector at Høvsøre and the marine site, the daily variation is different, with the variability of the mean wind speed following approximately the same pattern at all heights. The reversal height was estimated to be about 50 m at Høvsøre-coastal. At the marine site, FINO3, the maximum in the shape parameter was found at the lowest measuring level suggesting either a low reversal height or no reversal height at all.

The two terms in Eq. 4 weight the effect of surface diurnal stability cycle and the synoptic wind variability. The relative importance of the two terms is shown in Fig. 10, where term I (diurnal stability) dominates the profile in Hamburg up to 600 m, the maximum measurement height available in this study. At Høvsøre-land, term II (high altitude or synoptic variability)

Table 3 Parameters in Eq. 4 derived from least-squares fitting to the measurements

	z_s (m)	k_s	z_r (m)	z_t (m)	k_t	c	*RMSE* of fit
Hamburg	10	1.88	183	642	1.88	1.64	0.0274
Høvsøre land sector	10	2.33	118	1362	0.53	1.89	0.0207
Høvsøre Coastal sector	10	2.27	55	388	1.67	0.14	0.0219
FINO3 marine	5*	2.45*	15*	238	1.88	0.12	0.0058

* Values marked with * are outside the measuring range of the instruments and are estimated by fitting Eq. 4 to the value of k at 50 m

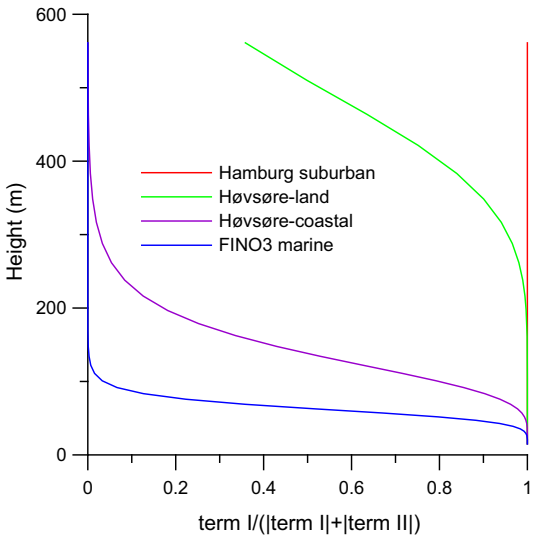

Fig. 10 Relative importance of term I in the parametrization of the shape parameter, Eq. 4

becomes noticeable at around 400 m, and is already significant at 100 m for the coastal sector at Høvsøre. Over the sea, term II dominates above 50 m, but this corresponds to the lowest observation height. When using the parametrization over the sea the reversal height was artificially set to 15 m due to the lack of any observations below 50 m, and to avoid a k profile with a zero gradient at the surface.

5.2 Reversal-Height Analysis

From Eq. 5, which provides a relationship between the normalized reversal height and surface Rossby number, and from the k profiles over land (Hamburg and Høvsøre-land), we derive the constant of proportionality α and investigate the sensitivity of the reversal height to changes in surface roughness. Due to considerable differences in the surface roughness between the sites, it is possible to estimate the sensitivity of the reversal height to surface roughness, expressed by the value of $1-\beta$ in Eq. 5. We take the ratio between the reversal heights at the two sites

$$\left(\frac{z_{r,\mathrm{Ha}}}{z_{r,\mathrm{H\o}}}\right) = \left(\frac{(G/f)_{\mathrm{Ha}}}{(G/f)_{\mathrm{H\o}}}\right)^{\beta} \left(\frac{z_{0,\mathrm{Ha}}}{z_{0,\mathrm{H\o}}}\right)^{1-\beta}, \tag{7}$$

Table 4 Measurements and parameters used to derive the constant of proportionality α between the normalized reversal height and the surface Rossby number, Eq. 5

	Wind speed at 600 m, G (m s^{-1})	Coriolis parameter f (s^{-1})	Reversal height z_r (m)	Roughness length z_0 (m)	α
Hamburg	12.2	1.17×10^{-4}	183	0.65	0.0058
Høvsøre land-sector	12.9	1.22×10^{-4}	118	0.014	0.0054
Høvsøre coastal sector	13.2	1.22×10^{-4}	55	0.014	0.0025

The value of β (0.9) was estimated from Eq. 7

where the subscripts Ha and $H\emptyset$ denote Hamburg and Høvsøre-land, respectively. Taking the observed mean wind speed at 600 m as representative of the geostrophic wind speed, using values of $z_0 = 0.65$ m and 0.014 m for Hamburg and Høvsøre-land, respectively, and taking z_r from Table 3, $1 - \beta$ is estimated to be 0.11. This is in good agreement with the value 0.1 suggested by Troen and Petersen (1989). It should be noted that the ratio $(G/f)_{\mathrm{Ha}} / (G/f)_{\mathrm{H\emptyset}}$ turns out to be very close to one and therefore is not sensitive to the value of β. From Eq. 5 and using the value $1 - \beta \approx 0.1$, $\alpha \approx 0.006$ for both Hamburg and the land sector at Høvsøre (Table 4). Thus, our estimate of α is considerably larger than 0.002, the value suggested by Troen and Petersen (1989).

Figure 9 shows that the reversal height at Høvsøre is much lower for flow from the sea than from land. The mast at Høvsøre is located 1.8 km from the shoreline, where the westerly flow is in transition between the upwind conditions over the sea and the downwind land conditions. The upper level of the transition layer constitutes the top of the internal boundary layer. Floors et al. (2011) found, from an analysis of measurements at Høvsøre, that the height of the internal boundary layer for momentum and wind velocity are different, in agreement with results from classical model simulations of the internal boundary layer, such as those of Rao et al. (1974) and Peterson (1969). It was found that the flow at Høvsøre was in full equilibrium with the land surface below 15 m; followed by a transition layer in which the wind velocity conforms to that over the sea; the top of this layer is at ≈80 m and above this the marine wind profile prevails although the momentum is still in a transition phase between sea and land conditions. This aspect of the internal boundary layer is illustrated in Floors et al. (2011) where the internal boundary layer at Høvsøre for momentum is about twice the height of the internal boundary layer for wind velocity.

Because the lowest part of the airflow in the internal boundary layer is in equilibrium with the land surface, it responds somewhat similarly to changes in atmospheric stability over land, while the upper part of the internal boundary layer is in transition. It is therefore reasonable to consider that the reversal height and the height of the internal boundary layer for velocity in the coastal zone are closely connected, and the growth of the internal boundary layer can be applied to predict the reversal height in the coastal zone. There are a multitude of applied models for the growth of the internal boundary layer (Melas and Kambezidis 1992; Gryning and Batchvarova 1990). For applied use, we here suggest the model of Troen and Petersen (1989) because it is easy to apply but, as pointed out by Floors et al. (2013), overestimates the height of the momentum internal boundary layer. Floors et al. (2011) found the height of the velocity internal boundary layer to be about one-third of the height of the internal boundary layer when estimated from the model in Troen and Petersen (1989), and half of the height for other models. Considering that the reversal height at Høvsøre for westerly wind directions is

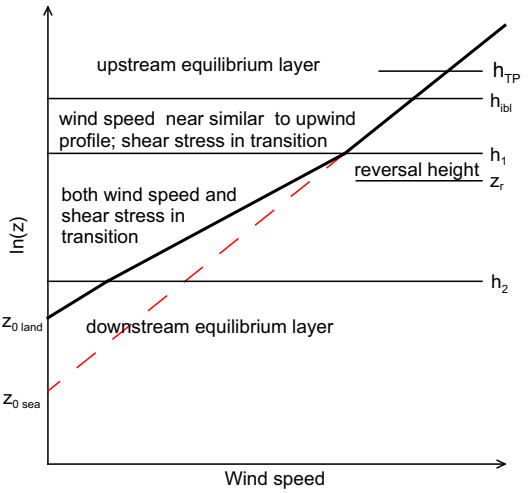

Fig. 11 Idealized illustration of the structure in the internal boundary layer (IBL) that develops overland downwind from a coastline: h_{TP}, height of the matching IBL following Troen and Petersen (1989); h_{ibl}, height of the momentum IBL; h_1, height of velocity IBL; h_2, height of the full equilibrium IBL; z_r, reversal height; $z_{0\,sea}$, sea-surface roughness; $z_{0\,land}$, land-surface roughness

lower (≈55 m) than the height of the velocity internal boundary layer (≈80 m) it is suggested that the reversal height is taken to be 0.25 of the height of the internal boundary layer when predicted by the model in Troen and Petersen (1989), $z_r \approx 0.25 h_{TP}$. For all other models the height of the velocity internal boundary layer is half and the reversal height 0.35 of the height of the momentum internal boundary layer, $z_r \approx 0.35 h_{ibl}$, (Fig. 11).

6 Discussion and Conclusions

Long-term measurements (9–11 month's duration) of the wind profile within the atmospheric boundary layer at an inland suburban site (Hamburg), a coastal site (Høvsøre) and a marine site (FINO3) have been analyzed. It is noted that the quality of the wind-speed measurements, when expressed in terms of *CNR* values, is generally higher in an environment that is influenced by the sea, likely due to sea spray, or the fact that humid conditions allow hygroscopic aerosol growth (note that the amount of backscattered signal is a function of both particle concentration and size). This is an important aspect for the use of lidars offshore. The best measurement conditions in this study (Fig. 3) are for onshore winds at Høvsøre where wave breaking caused by the shallow seabed and coastline acts as an additional source of particles in the marine air. Over land, the atmospheric particle concentration is generally less at the sites in question, indicated by the reduced *CNR* values.

It is observed that high *CNR* values are generally associated with high wind conditions. Over land such conditions cause suspension of particles from the ground and in the marine environment it also enhances the formation of marine aerosols, both processes increasing the background aerosol concentration and enhancing the backscatter signal. It should be mentioned that stagnation periods with low wind speeds over urban areas can also result in very high particle concentrations originating from anthropogenic pollutants, although this was not observed in the analysis of the Hamburg measurements.

Applying a high *CNR* threshold for filtering data results in a derived mean wind speed and reversal height that are both generally higher than when all data are used. In other words, applying high *CNR* threshold biases the climatology of wind profiles. Therefore, setting a *CNR* threshold should be done cautiously when creating wind-speed climatological profiles.

Gryning et al. (2014) applied a *CNR* threshold of –22 dB and found reversal heights larger than reported here, even though based on the same measurements.

Analysis of wind measurements over different surface types showed that, over land, the profile of the shape parameter has a maximum at a height of 100 to 200 m above the ground, depending mostly on the surface roughness. The analysis shows that the reversal height at the Høvsøre meteorological mast, which is 1.8 km from the coastline, is lower for flows from the sea than from the land sector; this is related to the development of an internal boundary layer. Over the sea at FINO3, the existence of a reversal height is not detected in the measurements down to 30 m, and it is clear that the conditions in which a reversal height develops over the sea are not fully understood and need further investigation.

A parametrization of the profile of the k-parameter suggested by Gryning et al. (2014) is applied to the data; it consists of two terms that describe the combination of the effect of surface-flux variability (term I in Eq. 4) and the synoptic-wind variability (term II in Eq. 4). The first term basically forms the elevated maximum in the k profile and is thus indispensable when the parametrization is used over land. This term loses significance in the k profile in coastal areas and its importance is further reduced over the sea, where term II becomes more important. At heights typical of wind turbines (100–150 m), the first term is essential for describing profiles over land; both terms are equally important for describing profiles in the coastal region where the reversal height is low, and the second term dominates k profiles in marine conditions.

It should be noted that the two-parameter Weibull distribution has been generally accepted for describing unimodal frequency distributions of wind speed at many sites and as a useful adequate tool for estimating the wind energy potential (Troen and Petersen 1989). However, the use of the Weibull distribution to describe the wind-speed probability is based on empirical rather than physical justifications and it is not always the most appropriate distribution for the measurements (Tuller and Brett 1984; Drobinski et al. 2015). For practical use, a less appealing, but theoretically better justified distribution, has been suggested by Sardeshmukh and Sura (2009).

Acknowledgments The study was supported by the Danish Council for Strategic Research, project number 2104-08-0025 named "Tall Wind", and the Nordic Centre of Excellence Program CRAICC. The work is related to activities of two of the authors (SEG and EB) within the TOPROF COST Action ES1303. The measurements from the M2 mast were kindly made available by Vattenfall and DONG Energy, and those from the mast at the FINO3 research platform by the BMU (Bundesministerium für Umwelt, German Federal Ministry for the Environment, Nature Conservation and Nuclear Safety) and the PTJ (Projektträger Jülich, project executing organisation). We thank the Test and Measurements section of DTU Wind Energy for maintenance of the Høvsøre database, and Ewan O'Connor who kindly read through the manuscript.

References

Aitkin ML, Rhodes ME, Lundquist JE (2012) Performance of a wind-profiling lidar in the region of wind turbine rotor disks. J Atmos Ocean Technol 29:347–355

Batchvarova E, Gryning SE, Skov H, Sørensen LL, Kirova H, Münkel C (2014) Boundary-layer and air quality study at "Station Nord" in Greenland. In: Steyn D, Mahur R (eds) Air pollution modelling and its application XXIII. Springer International Publishing, Cham, pp 525–529

Bickel PJ, Doksum KA (2001) Mathematical statistics, basic ideas and selected topics, vol 1, 2nd edn. Pearson, Prentice Hall, 576 pp
Blatt A (2010) Roughness length analysis for wind energy purposes. Technical Report master Thesis, Risø DTU, Roskilde, 114 pp
Brümmer B, Lange I, Konow H (2012) Atmospheric boundary layer measuremenst at the 280 m high Hamburg weather mast 1995–2011: mean annual and diurnal cycles. Meteorol Z 21(4):319–335
Brümmer B, Schultze M (2015) Analysis of a 7-year low-level temperature inversion data set measured at 280 m high Hamburg weather mast. Meteorol Z PrePub. doi:10.1127/metz/2015/0669
Cariou JP (2013) Pulsed lidars. In: Peña A, Hasager CB, Lange J, Anger J, Badger M, Bingöl F, Bischoff O, Cariou JP, Dunne F, Emeis S, Harris M, Hofsäss M, Karagali I, Laks J, Larsen S, Mann J, Mikkelsen T, Pao LY, Pitter M, Rettenmeier A, Sathe A, Scanzani F, Schlipf D, Simley E, Slinger C, Wagner R, Würth I (eds) Remote sensing for wind energy. DTU Wind Energy-E-Report-0029(EN), pp 104–121
Coleman TF, Li Y (1996) An interior, trust region approach for nonlinear minimization subject to bounds. SIAM J Optim 6:418–445
Doran JC, Verholek MG (1978) A note on vertical extrapolation formulas for Weibull velocity distribution parameters. J Appl Meteorol 17:410–412
Drobinski P, Coulais C, Jourdier B (2015) Surface wind-speed statistics modelling: alternatives to the Weibull distribution and performance evaluation. Boundary-Layer Meteorol 157:97–123
Floors R (2010) Analysis of diabatic flow modification in the internal boundary layer. Master Thesis at Wageningen University, Meteorology and Air Quality Group, 51 pp
Floors R (2013) Measuring and modelling of the wind on the scale of tall wind turbines. DTU Wind Energy PhD-0034(EN) report
Floors R, Gryning SE, Peña A, Batchvarova E (2011) Analysis of diabatic flow modifications in the internal boundary layer. Meteorol Z 20(6):649–659
Floors R, Vincent C-L, Gryning SE, Peña A, Batchvarova E (2013) The wind profile in the coastal boundary layer: wind lidar measurements and numerical modelling. Boundary-Layer Meteorol 147:469–491
Frehlich R (1996) Simulation of coherent Doppler lidar performance in the weak-signal regime. J Atmos Ocean Technol 13:646–658
Fujii Y, Yamashita J, Shikata S, Saito S (1978) Incoherent optical heterodyne detection and its application to air pollution detection. Appl Opt 17:3444–3449
Fujii T, Fukuchi T (2005) Laser Remote Sensing. Taylor & Francis Group, Boca Raton, 912 pp
Gryning SE, Lyck E (1984) Atmospheric dispersion from elevated sources in an urban area: comparison between tracer experiments and model calculations. J Clim Appl Meteorol 23:651–660
Gryning SE, Batchvarova E (1990) Analytical model for the growth of the coastal internal boundary layer during onshore flow. Q J R Meteorol Soc 116:187–203
Gryning SE, Batchvarova E, Brümmer B, Jørgensen H, Larsen S (2007) On the extension of the wind profile over homogeneous terrain beyond the surface boundary layer. Boundary-Layer Meteorol 124:251–268
Gryning SE, Batchvarova E, Floors R, Peña A, Brümmer B, Hahmann AN, Mikkelsen T (2014) Long-term profiles of wind and Weibull distribution parameters up to 600 m in a rural coastal and an inland suburban area. Boundary-Layer Meteorol 150:167–184
Hellmann G (1917) Über die bewegung der luft in den unteren schichten der atmosphäre. Meteorol Z 34:273–285
Justus CG, Mikhail A (1976) Height variation of wind speed and wind distributions statistics. Geophys Res Lett 3(3):261–264
Justus CG, Hargraves WR, Mikhael A, Graber D (1978) Methods for estimating wind speed frequency distributions. J Appl Meteorol 17:350–353
Konow H (2014) Tall wind profiles in heterogeneous terrain. PhD Thesis, University of Hamburg, 107 pp
Melas D, Kambezidis HD (1992) The depth of the internal boundary layer over an urban area under sea-breeze conditions. Boundary-Layer Meteorol 61:247–264
O'Connor EJ, Illingworth AJ, Brooks IM, Westbrook CD, Hogan RJ, Davies F, Brooks BJ (2010) A method for estimating the turbulent kinetic energy dissipation rate from a vertically-pointing Doppler lidar, and independent evaluation from balloon-borne in-situ measurements. J Atmos Ocean Technol 27:1652–1664
Peña A, Gryning SE, Hahmann AN (2013) Observations of the atmospheric boundary layer height under marine upstream flow conditions at a coastal site. J Geophys Res 118:1924–1940
Peña A, Floors R, Sathe A, Gryning SE, Wagner R, Courtney MS, Lársen XG, Hahmann AN, Hasager CB (2015a) Ten years of boundary-layer and wind-power meteorology at Høvsøre, Denmark. Boundary-Layer Meteorol. doi:10.1007/s10546-015-0079-8
Peña A, Floors R, Gryning SE (2015b) Reply on the comment by Bergman on "The Høvsøre Tall Wind-Profile Experiment: A Description of Wind Profile Observations in the Atmospheric Boundary Layer". Boundary-Layer Meteorol. doi:10.1007/s10546-015-0077-x

Petersen EL (1975) On the kinetic energy spectrum of atmospheric motions in the planetary boundary layer. Risø National Laboratory, Risoe-R 285, 103 pp
Peterson EW (1969) Modification of mean flow and turbulent energy by a change in surface roughness under conditions of neutral stability. Q J R Meteorol Soc 95:561–575
Rao KS, Wyngaard JC, Cote OR (1974) The structure of the two-dimensional internal boundary layer over a sudden change of surface roughness. J Atmos Sci 31:738–746
Sardeshmukh PD, Sura P (2009) Reconciling non-Gaussian climate statistics with linear dynamics. J Clim 22:1193–1207
Sathe A, Gryning SE, Peña A (2011) Comparison of the atmospheric stability and wind profiles at two wind farm sites over a long marine fetch in the North Sea. Wind Energy 14:767–780
Suomi I, Gryning SE, Floors R, Vihma T, Fortelius C (2015) On the vertical structure of wind gusts. Q J R Meteorol Soc 141:1658–1670
Troen I, Petersen EL (1989) European Wind Atlas. Risø National Laboratory, Roskilde. ISBN 87-550-1482-8, 656 pp
Tuller SE, Brett AC (1984) The characteristics of wind velocity that favor the fitting of a Weibull distribution in wind speed analysis. J Clim Appl Meteorol 23:124–134
Vincent CL, Hahmann AN, Kelly MC (2012) Idealized mesoscale model simulations of open cellular convection over the sea. Boundary-Layer Meteorol 142:103–121
Wieringa J (1989) Shapes of annual frequency distribution of wind speed observed on high meteorological masts. Boundary-Layer Meteorol 47:85–110
Zimmer RP, Justus CG, Mason RM, Robinette SL, Sassone PG, Schaffer WA (1975) Benefit-cost methodology study with example application of the use of wind generators. NASA CR-134864